1521-0111/88/6/1035–1044$25.00
MOLECULAR PHARMACOLOGY

http://dx.doi.org/10.1124/mol.115.101444
Mol Pharmacol 88:1035–1044, December 2015

Nicotine Dependence Reveals Distinct Responses from Neurons and Their Resident Nicotinic Receptors in Medial Habenula

Pei-Yu Shih, J. Michael McIntosh, and Ryan M. Drenan

Department of Medicinal Chemistry and Molecular Pharmacology, Purdue University, West Lafayette, Indiana (P.-Y.S., R.M.D.) and George E. Wahlen Veterans Affairs Medical Center and Departments of Psychiatry and Biology, University of Utah, Salt Lake City, Utah (J.M.M.)

Received August 19, 2015; accepted September 30, 2015

ABSTRACT

Nicotinic acetylcholine receptors (nAChRs) are the molecular target of nicotine. nAChRs in the medial habenula (MHb) have recently been shown to play a role in nicotine dependence, but it is not clear which nAChR subtypes or MHb neuron types are most important. To identify MHb nAChRs and/or cell types that play a role in nicotine dependence, we studied these receptors and cells with brain slice electrophysiology using both acute and chronic nicotine application. Cells in the ventroinferior (MHbVI) and ventrolateral MHb (MHbVL) subregions expressed functional nAChRs with different pharmacology. Further, application of nicotine to cells in these subregions led to different action potential firing patterns. The latter result was correlated with a differing ability of nicotine to induce nAChR desensitization. Chronic nicotine caused functional upregulation of nAChRs selectively in MHbVI cells, but did not change nAChR function in MHbVL. Importantly, firing responses were also differentially altered in these subregions following chronic nicotine. MHbVI neurons treated chronically with nicotine exhibited enhanced basal pacemaker firing but a blunted nicotine-induced firing response. MHbVL neurons did not change their firing properties in response to chronic nicotine. Together, these results suggest that acute and chronic nicotine differentially affect nAChR function and output of cells in MHb subregions. Because the MHb extensively innervates the interpeduncular nucleus, an area critical for both affective and somatic signs of withdrawal, these results could reflect some of the neurophysiological changes thought to occur in the MHb to the interpeduncular nucleus circuit in human smokers.

Introduction

Chronic exposure to nicotine in tobacco products results in numerous health consequences (lung cancer, emphysema, hypertension, etc.) and accounts for over 6 million deaths per year (World Health Organization, 2011). Nicotine is the primary psychoactive substance in tobacco products, and it is addictive due to its ability to strongly activate neuronal nicotinic acetylcholine receptors (nAChRs) (Steinsland and Furchgott, 1975). It has recently been appreciated that long-term nicotine use is maintained via a balanced activation of brain circuits mediating both positive (rewarding) and negative (aversive) motivational signals (Matsumoto and Hikosaka, 2007, 2009; Bromberg-Martin et al., 2010; Hikosaka, 2010). It is also established that chronically exposing the brain to nicotine changes nAChR number and/or function in key brain circuits (Marks et al., 1983; Lester et al., 2009). These alterations in nAChR function and the consequent changes in neuronal circuit activity where these receptors reside are among the key events important for establishing and maintaining addiction to nicotine. Positive motivational signals generated by nicotine use the mesolimbic dopamine pathway, and much has been learned regarding this system (Laviolette and van der Kooy, 2004; Dani and Harris, 2005; Dani and Bertrand, 2007). By contrast, relatively little is known about the nAChRs and brain circuits mediating nicotine's aversive quality. In this study, we sought to study one of the key brain areas mediating negative motivational signals after nicotine use: the medial habenula (MHb).

The MHb is a small bilateral structure immediately ventral to the hippocampus and adjacent to the third ventricle. The MHb sends a prominent projection via the fasciculus retroflexus to a midline structure in the ventral midbrain: the interpeduncular nucleus (IPN). Via the MHb's connection to areas such as the septum and nucleus of diagonal band (Herkenham and Nauta, 1977; Qin and Luo, 2009) and the IPN's connection to the raphe (Shibata and Suzuki, 1984; Montone et al., 1988), the MHb to IPN pathway is a key circuit connecting forebrain structures with midbrain areas important for motivation and reward. The MHb to IPN pathway is a crucial mediator of nicotine withdrawal following chronic exposure to nicotine, and specific nAChRs play a key role.

This work was supported by the National Institutes of Health [Grant DA030396], Brain and Behavior Research Foundation (via a NARSAD Young Investigator Award), Ralph W. and Grace M. Showalter Research Trust, and Purdue University.
dx.doi.org/10.1124/mol.115.101444.

ABBREVIATIONS: ACh, acetylcholine; ANOVA, analysis of variance; BAC, bacterial artificial chromosome; ChAT, choline acetyltransferase; αCtxMII, α-conotoxin MII; DHβE, dihydro-β-erythroidine; IPN, interpeduncular nucleus; MHb, medial habenula; MHbVI, ventroinferior medial habenula; MHbVL, ventrolateral medial habenula; nAChR, nicotinic acetylcholine receptor; PBS, phosphate-buffered saline; PBST, phosphate-buffered saline containing 10% normal horse serum, 2% bovine serum albumin, and 0.3% Triton X-100; VTA, ventral tegmental area; WT, wild type.

For example, mice lacking $\alpha5$ and $\beta4$ subunits, which are expressed in the MHb or IPN, exhibit reduced withdrawal responses when chronic nicotine is removed (Salas et al., 2004, 2009). Similarly, antagonizing nAChRs via infusion of pharmacological blockers into the MHb also reduces the severity of nicotine withdrawal (Salas et al., 2009). Mice lacking $\alpha5$ subunits self-administer greater amounts of nicotine (i.e., they have reduced aversive signals at high doses of nicotine), and self-administration is normalized when $\alpha5$ subunits are reintroduced into the MHb (Fowler et al., 2011). Conversely, transgenic mice overexpressing nAChRs in MHb show enhanced sensitivity to the aversive aspects of nicotine (Frahm et al., 2011).

Although these early and seminal studies clearly demonstrate the importance of MHb nAChRs in the motivational response to nicotine, a detailed picture elucidating specific nAChRs in specific MHb neurons has not yet emerged. Both classic and recent studies have determined that the MHb is not a homogeneous structure, but is rather a collection of diverse cell types that could have varied physiologic actions. For example, several MHb subnuclei exist that each contain neuron types expressing various biochemical markers (Aizawa et al., 2012). Cells in the dorsal 1/3 of the MHb preferentially express substance P, whereas cells in the ventral 2/3 of the MHb preferentially express choline acetyltransferase (ChAT), a cholinergic marker (Contestabile et al., 1987; Yamaguchi et al., 2013). The dorsal and ventral MHb project to anatomically divergent components of the IPN (Contestabile and Flumerfelt, 1981; Yamaguchi et al., 2013; Shih et al., 2014), and different regions of IPN have recently been appreciated to mediate diverse aspects of nicotine withdrawal. For example, the dorsal IPN, which receives projections from the ventrolateral MHb (MHbVL), is a key mediator of the somatic aspect of nicotine withdrawal (Zhao-Shea et al., 2013). Further, areas in the ventral IPN, which receive projections preferentially from ventroinferior MHb (MHbVI), appear to more strongly control affective signs of nicotine withdrawal (Zhao-Shea et al., 2015). These recent data point to the need for a more thorough description of the nAChRs in different subnuclei of MHb. In this study, we used brain slice patch clamp electrophysiology, pharmacology, and genetics to examine nAChR function in MHbVI and MHbVL. We present evidence demonstrating that nAChRs in different MHb subregions respond differently to acute and chronic nicotine, which in turn differentially affect neuronal activity in these areas.

Materials and Methods

Animals. All procedures involving the use of live animals conformed to the guidelines provided by the National Institutes of Health Office of Laboratory Animal Welfare. All protocols were approved by the Purdue University Institutional Animal Care and Use Committee. Mice were housed at 22°C, with an alternating 12-hour light/dark cycle. Food and water was available ad libitum. Mice were weaned and group housed with same sex littermates at postnatal day 21. Adult (2–3 months old) mice were used for this study. No gender-based differences were noted, so male and female data were pooled for subsequent analyses.

Most studies were conducted with C57BL/6 wild-type (WT) mice obtained from Jackson Laboratories (Bar Harbor, ME). Select experiments used genetically modified mice. $\alpha4$ knockout ($\alpha4$KO) mice were a generous gift of Drs. Michael Marks and Jerry Stitzel (University of Colorado, Boulder, CO) and were produced by mating mice heterozygous for the $\alpha4$KO allele. $\alpha6$L9S mice were generated as previously described (Drenan et al., 2008). A Leu "9-prime" to Ser mutation was introduced into a bacterial artificial chromosome (BAC) at the $\alpha6$ nAChR subunit gene. Mutant BAC DNA was injected into FVB/N embryos, and the embryos were implanted into pseudopregnant Swiss-Webster surrogates. The transgene insertion site in the mouse genome is unknown. Founder animals were identified and backcrossed to C57BL/6 mice for 12 or more generations. As a result, 90–95% of the genome of the $\alpha6$L9S strain is expected to be C57BL/6. FVB/N allelic DNA close to the insertion site is likely to persist. The L9S mutation leaves $\alpha6$* nAChRs 10- to 100-fold more sensitive to ligands compared with non$-\alpha6$* nAChRs (Drenan et al., 2008, 2010; Cohen et al., 2012). Previous studies have confirmed that $\alpha6$* nAChRs are not overexpressed or expressed in ectopic brain regions in $\alpha6$L9S mice (Drenan et al., 2008, 2010). Littermate mice not harboring the mutant BAC served as controls for $\alpha6$L9S mice in electrophysiology experiments. Mutant mouse lines were genotyped by polymerase chain reaction analysis of isolated tail DNA as previously described (Drenan et al., 2008).

Brain Slice Preparation. Mice were anesthetized with sodium pentobarbital (100 mg/kg i.p.) and transcardially perfused with 4°C *N*-methyl-D-glucamine–based recovery solution (in mM: 93 *N*-methyl-D-glucamine, 2.5 KCl, 1.2 NaH_2PO_4, 30 $NaHCO_3$, 20 HEPES, 25 glucose, 5 Na-ascorbate, 2 thiourea, 3 Na-pyruvate, 10 $MgSO_4{\cdot}7H_2O$, and 0.5 $CaCl_2{\cdot}2H_2O$). Brains were removed and 200-μm-thick coronal slices containing the MHb were prepared with a vibrating microslicer (DTK Zero 1; Ted Pella, Redding, CA). Slices were allowed to recover for 12 minutes at 33°C and then at room temperature for 1–8 hours in HEPES-holding solution (in mM: 92 NaCl, 2.5 KCl, 1.2 NaH_2PO_4, 30 $NaHCO_3$, 20 HEPES, 25 glucose, 5 Na-ascorbate, 2 thiourea, 3 Na-pyruvate, 2 $MgSO_4{\cdot}7H_2O$, and 2 $CaCl_2{\cdot}2H_2O$). All solutions were saturated with 95% O_2 and 5% CO_2, with osmolarity adjusted to 300–310 mOsm.

Patch Clamp Electrophysiology. Each individual slice was transferred to a recording chamber and was continuously superfused at a rate of 2–3 ml/min at 30–32°C (Warner Instrument, Hamden, CT), with standard recording artificial cerebrospinal fluid (in mM: 124 NaCl, 2.5 KCl, 1.2 NaH_2PO_4, 24 $NaHCO_3$, 12.5 glucose, 2 $MgSO_4{\cdot}7H_2O$, and 2 $CaCl_2{\cdot}2H_2O$). MHb neurons were visually identified under infrared illumination using a Nikon FN-1 microscope equipped with differential interference contrast optics and a water-immersion objective lens (40×, numerical aperture = 0.8; Nikon, Tokyo, Japan). MHb cell recordings were obtained from either the MHbVI area close to the third ventricle or the MHbVL area adjacent to the lateral habenula (Fig. 1A). Whole-cell recordings and cell-attached recordings were obtained with patch pipettes filled with internal solution (in mM: 135 K-gluconate, 5 EGTA, 10 HEPES, 2 MgATP, 0,1 NaGTP, 0.5 $CaCl_2$, and 2 $MgCl_2$, pH adjusted to 7.3 with Tris base). In a subset of experiments, 2.5 mg/ml biocytin was added to the internal solution to mark the recorded neuron for later cytochemical characterization. Data were collected using a Multiclamp 700B amplifier (Molecular Devices, Sunnyvale, CA), filtered at 2 kHz, and sampled at 10 kHz by a Digidata 1440A digitizer (Molecular Devices). Series resistance was measured by injection of hyperpolarizing pulses (−5 mV, 100 milliseconds) and was not compensated. To examine the functional nAChR response, acetylcholine (ACh) was locally applied (250 milliseconds, 12 psi) at different concentrations (1–100 μM) using a glass pipette connected to a PV-820 Pneumatic Picopump (World Precision Instruments, Inc., Sarasota, FL). This pipette was moved to within 20–40 μm of the recorded cell with a piezoelectric manipulator (PA-100/12; Piezosystem Jena, Hopedale, MA) for drug application and retracted after the end of the puff to minimize nAChR desensitization. All other drugs were bath perfused at final concentrations indicated by diluting aliquots of stock solution in artificial cerebrospinal fluid.

Immunohistochemistry. To identify the location of recorded cells, slices containing biocytin-loaded cells were fixed by immersion in 4% paraformaldehyde in phosphate-buffered saline (PBS) overnight at 4°C. Sections were washed 2 times for 10 minutes per wash in PBS,

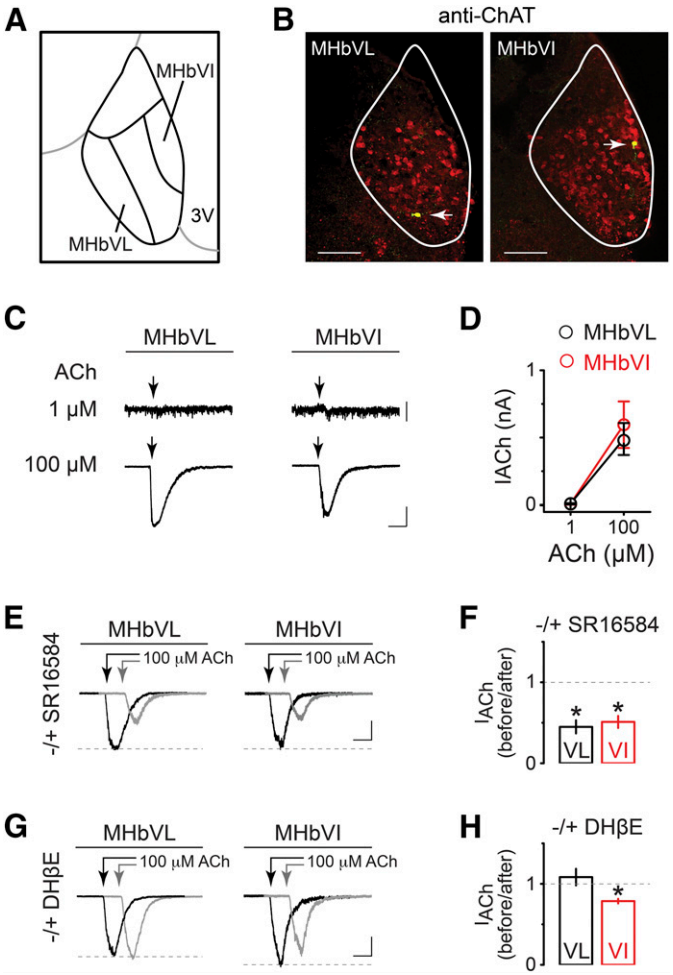

Fig. 1. Functional differences in nAChRs between MHbVL and MHbVI neurons. (A) Schematic diagram defining a third of the ventrolateral portion of MHb as MHbVL and a third of the ventroinferior portion of MHb as MHbVI. (B) Locations of recorded cells in MHbVL and MHbVI were visualized by intracellular biocytin staining (green) and immunostaining for ChAT (red). Yellow cells (white arrow) are double-labeled cells. Representative data from labeled cells in MHbVL (left panel) and MHbVI (right panel) are shown. Scale bar: 100 μm. (C) Examples of currents evoked by 1 and 100 μM acetylcholine (250-millisecond puffs) in MHbVL. Scale bar: 10 pA (1 μM ACh) and 200 pA (100 μM ACh), 500 milliseconds. (D) Summary plot of peak ACh-evoked currents at the indicated concentrations in MHbVL and MHbVI neurons. (E) Representative traces showing 100 μM ACh-induced current before (black trace) and 15 minutes after (gray trace; offset for clarity) application of SR16584 (20 μM). Arrows indicate ACh applications. Scale bar: 250 pA, 350 milliseconds (MHbVL); 150 pA, 350 milliseconds (MHbVI). (F) Summary bar graphs are plotted to indicate the degree of inhibition (i.e., the fraction of control current remaining after application of SR16584); $^*p < 0.05$ (paired t test). (G) Representative traces showing 100 μM ACh-induced current before (black trace) and 15 minutes after (gray trace; offset for clarity) application of DHβE (500 nM). Arrows indicate ACh applications. Scale bar: 250 pA, 350 milliseconds (MHbVL); 200 pA, 350 milliseconds (MHbVI). (H) Summary bar graphs are plotted to indicate the degree of inhibition (i.e., the fraction of control current remaining after application of DHβE); $^*p < 0.05$ (paired t test).

blocked, and permeabilized for 60 minutes in PBS containing 10% normal horse serum, 2% bovine serum albumin, and 0.3% Triton X-100 (PBST). Primary antibody incubations were done overnight at 4°C in PBST containing goat anti-ChAT (1:500; Millipore, Billerica, MA) and streptavidin conjugated Alexa-488 (1:1000; Thermo Fisher, Waltham, MA). After three PBS washes, secondary antibody incubations were performed for 2 hours at room temperature in PBST containing Alexa-555 donkey–anti-goat (1:500; Invitrogen). Sections were finally washed 3 times for 10 minutes per wash, mounted with antifade mounting medium (Vectashield; Vector Laboratories, Burlingame, CA), and coverslipped for confocal microscopy.

Chronic Nicotine Treatment. Nicotine dependence was induced with osmotic minipumps (model 2004; Alzet, Cupertino, CA) as previously reported (Shih et al., 2014). These minipumps, implanted subcutaneously under brief isoflurane anesthesia, were filled with either sterile saline or (–)-nicotine hydrogen–tartrate salt (Glentham Life Sciences, Corsham, UK) dissolved in sterile saline. Mice received a mean dose of 1 mg/kg per hour of nicotine for 14 days. The nicotine dose used in this study to develop physical dependence was chosen based on the results obtained in previous studies (Matta et al., 2007; Hilario et al., 2012; Shih et al., 2014). This dose yields plasma levels of ~0.3 μM, a concentration similar to that observed in human smokers consuming an average of 17 cigarettes a day (Matta et al., 2007).

Data Analysis and Statistical Methods. Off-line data analysis was performed using Clampfit 10 (Molecular Devices), GraphPad Prism 6 (GraphPad Software, La Jolla, CA), and Origin 9.0 (Originlab, Northampton, MA). Summary data are reported as mean ± S.E.M. Statistical significance was assessed by two-tailed paired t tests to assess the effect of a drug within a recorded neuron and unpaired t test to compare across neurons. One-way analysis of variance (ANOVA) followed by Tukey's post hoc tests was applied for multiple comparisons. Differences were considered statistically significant at $p < 0.05$.

Chemicals. All reagents were made from 1000× stock solutions kept frozen at −20°C in 50–100 μl aliquots. 6-Cyano-7-nitroquinoxaline-2,3-dione was purchased from Tocris (Bristol, UK). α-Conotoxin MII was synthesized as described previously (Azam et al., 2010). Unless specified otherwise, all other chemicals were purchased from Sigma-Aldrich (St. Louis, MO).

Results

In our previous study, we developed a map of nAChR subunit expression and localization within MHb. We noted that the α4, α6, β2, and β3 subunits exhibit a localization gradient from inferior to lateral across the ventral portion of MHb. In particular, α4 subunits are concentrated in MHbVL and α6 subunits are preferentially confined to MHbVI (Shih et al., 2014). Given that the patterns seen for various nAChR subunits suggest that specific subdivisions exist in MHb, we first sought to determine whether nAChRs in MHbVL and MHbVI exhibit functional differences. To compare the ACh sensitivity in MHbVL and MHbVI, we performed whole-cell patch recordings from visually identified cells in these two subregions. Our definition of MHbVI and MHbVL follows that of a recent study (Aizawa et al., 2012). MHbVL cells are located in the lateral one-third of the ventral MHb, mostly along the border between MHb and the lateral habenula. MHbVI cells are located in the inferior one-third of the ventral MHb, adjacent to the third ventricle (Fig. 1A). To further verify the location of recorded cells, a subset of cells was filled with biocytin during recordings, followed by post hoc identification using immunostaining and confocal microscopy. ChAT costaining was used to label the boundary of the ventral MHb (Fig. 1B) (Contestabile et al., 1987).

To study nAChR function, local pressure application was used to apply brief (250 millisecond) pulses of ACh from glass micropipettes positioned approximately 20–40 μm from the recorded cells using a piezoelectric translator as previously described (Engle et al., 2013). A low concentration of ACh (1 μM) evoked small inward currents or a zero current at a holding potential of −60 mV (Fig. 1, C and D), irrespective of the location of the cells (MHbVL: 9.1 ± 3.1 pA, $n = 6$; MHbVI:

7.5 ± 3.4 pA, $n = 4$, $p = 0.7460$). Application of 100 μM ACh induced currents of similar peak amplitude in MHbVL and MHbVI neurons (Fig. 1, C and D) (MHbVL: 489.0 ± 118.8 pA, $n = 6$; MHbVI: 597.9 ± 172.9 pA, $n = 4$, $p = 0.6310$). These findings indicate that neurons in MHbVL and MHbVI have roughly equal sensitivity to puff-applied 1 and 100 μM ACh. MHb neurons are highly enriched in mRNAs for most nAChR subunits (Marks et al., 1992).

Immunoprecipitation and immunopurification studies revealed a wealth of uncommon nAChR subtypes in MHb (Grady et al., 2009). The nAChRs expressed in MHb can be grouped to two major and distinct nAChR populations: β2- and β4-containing nAChRs (β2* and β4*; the asterisk indicates other unidentified subunits may coassemble with the indicated subunits). Next, we sought to determine which nAChR subtype(s) is/are responsible for the ACh-induced currents we measured in MHbVL and MHbVI. First, we tested whether ACh-induced currents in MHbVL and MHbVI could be blocked by the $\alpha3\beta4$* nAChR antagonist SR16584 (20 μM). Application of SR16584 resulted in a significant blockade of ACh-induced currents in both MHbVL (Fig. 1, E and F; $n = 6$, 44.9 ± 8.1% remaining response, $p = 0.0223$) and MHbVI areas (Fig. 1, E and F; $n = 5$, 51.0 ± 7.4% remaining response, $p = 0.0141$). Next, we tested dihydro-β-erythroidine (DHβE), which is traditionally used to discriminate β2* nAChRs from homomeric α7 nAChRs. We applied ACh (100 μM) with a puff electrode for 250 milliseconds and repeated this procedure after a 15-minute exposure to DHβE (500 nM). ACh-induced currents in MHbVL were not influenced by DHβE exposure (Fig. 1, G and H; $n = 5$, 108.0 ± 10.2% remaining response, $p = 0.5568$). In contrast, ACh-induced currents in MHbVI neurons were partially inhibited after application of DHβE (Fig. 1, G and H; $n = 5$, 78.7 ± 2.9% remaining response, $p = 0.0196$). These data show that pharmacologically distinct nAChRs exist in MHbVL and MHbVI.

Our previous studies strongly suggest that functional α6* nAChRs are expressed in MHbVI (Henderson et al., 2014; Shih et al., 2014). We conducted further pharmacological experiments to test this hypothesis. α-Conotoxin MII (αCtxMII), a cone snail toxin, is an antagonist with selectivity for α6* and α3* nAChRs. In particular, αCtxMII is 5.6-fold more selective for α6* versus α3* nAChRs, with little activity at other nAChR subtypes (Cartier et al., 1996; McIntosh et al., 2004). We measured ACh (100 μM) evoked current amplitudes in MHbVL and MHbVI neurons before and after bath application of 100 nM αCtxMII. Interestingly, αCtxMII did not significantly affect responses to 100 μM ACh in either MHb subregion (Fig. 2, A and B; MHbVL: 102.3 ± 5.6% remaining response, $n = 4$, $p = 0.8332$; MHbVI: 108.7 ± 14.2% remaining response, $n = 8$, $p = 0.8793$). α6* nAChRs in the dopamine pathway are known to exhibit high sensitivity to ACh and nicotine (Salminen et al., 2007) so we reasoned that if functional MHb α6* nAChRs exist, they may also exhibit high ACh sensitivity. We therefore tested the ability of αCtxMII to block currents evoked by lower concentrations of ACh, as the large currents evoked by 100 μM ACh (~500 pA) could preclude us from effectively isolating a small, αCtxMII-sensitive response. In MHbVI neurons, 10 μM ACh reliably evoked inward currents of 50–75 pA (Fig. 2C; 63.0 ± 13.1 pA, $n = 9$). An αCtxMII bath application resulted in a significant inhibition of inward currents evoked by 10 μM ACh in seven of nine MHbVI cells tested (Fig. 2, C and D; 51.6 ± 4.7% remaining response, $p = 0.0085$). In MHbVL neurons, 10 μM ACh was insufficient to evoke workable inward currents, but a 30 μM ACh application did result in measurable currents (Fig. 2C; 79.8 ± 10.4 pA, $n = 5$). However, αCtxMII was unable to block or attenuate inward currents evoked by 30 μM ACh in any of the MHbVL cells tested (Fig. 2, C and D; 103.7 ± 13.9% remaining response, $p = 0.8286$). These results suggest that MHbVI neurons express a high-sensitivity nAChR subtype, with sensitivity to αCtxMII.

To further test the hypothesis that the αCtxMII-sensitive nAChR subtype we identified in MHbVI neurons contains α6 subunits, we studied functional nAChR responses in α6L9S mice. α6L9S mice are a transgenic mouse strain harboring a bacterial artificial chromosome that directs expression of an α6 nAChR subunit, with a Leu to Ser mutation at a conserved residue in the second transmembrane α-helix (Drenan et al., 2008). This mutation renders α6* nAChRs "hypersensitive" to

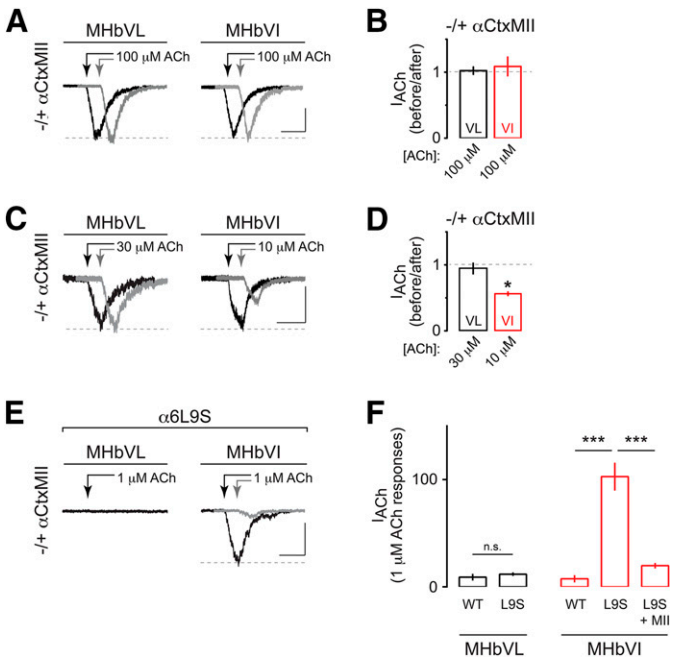

Fig. 2. Functional α6* nAChR expression is specific to MHbVI. (A) Representative traces showing 100 μM–induced currents in MHbVL and MHbVI neurons before (black trace) and 15 minutes after (gray trace; offset for clarity) application of αCtxMII (100 nM). Arrows indicate ACh applications. Scale bar: 100 pA, 500 milliseconds (MHbVL); 90 pA, 500 milliseconds (MHbVI). (B) Summary bar graphs to indicate the degree of inhibition by αCtxMII (i.e., the fraction of control current remaining after application of αCtxMII) for ACh-evoked responses in MHbVL and MHbVI neurons. (C) Representative traces showing 30 μM (for MHbVL neurons) or 10 μM (for MHbVI neurons) ACh-evoked currents before (black trace) and after (gray trace; offset for clarity) application of αCtxMII (100 nM). Different ACh concentrations were used in MHbVL versus MHbVI based on the minimum ACh concentration that evoked workable inward currents. Scale bar: 50 pA, 500 milliseconds (MHbVL); 60 pA, 500 milliseconds (MHbVI). (D) Summary bar graphs to indicate the degree of inhibition by αCtxMII (i.e., the fraction of control current remaining after application of αCtxMII) for 30 μM (MHbVL) or 10 μM (MHbVI) ACh-evoked responses; $^*p < 0.05$ (paired t test). (E) Representative traces for 1 μM ACh-evoked currents in MHbVL and MHbVI cells in slices from α6L9S mice. MHbVI cells, which responded robustly to 1 μM ACh (black trace), were subsequently exposed to αCtxMII (100 nM), and 1 μM ACh-evoked currents were measured in the presence of αCtxMII (gray trace). Scale bar: 70 pA, 500 milliseconds. (F) Summary bar graphs to indicate the average 1 μM ACh-evoked current response amplitude in MHbVL and MHbVI neurons in slices from α6L9S and nontransgenic control littermate (WT) mice; $^{***}p < 0.001$ (one-way ANOVA, Tukey's post hoc test).

agonists, such as nicotine and ACh. By puff applying low concentrations of ACh, α6* nAChRs can be selectively activated (Drenan et al., 2008; Engle et al., 2012, 2013; Powers et al., 2013). This is a helpful method for determining whether a particular cell type in the brain expresses functional α6* nAChRs. We therefore studied MHbVL and MHbVI neurons in α6L9S mice. Whereas MHbVL neurons did not respond appreciably to low (1 μM) concentrations of ACh (Fig. 2, E and F; 11.9 ± 1.7 pA, $n = 7$), MHbVI neurons in slices from α6L9S mice responded with robust inward currents following application of 1 μM ACh (Fig. 2, E and F; 102.8 ± 13.0 pA, $n = 8$; ANOVA: $F_{(4,25)} = 30.05$, $p < 0.0001$; Tukey's post hoc test: $p < 0.001$ versus WT). Further, ACh (1 μM) evoked currents in α6L9S MHbVI neurons were substantially blocked by bath application of αCtxMII (Fig. 2, E and F; 20.4 ± 3.0% remaining response, $n = 5$; Tukey's post hoc test: $P < 0.001$ versus α6L9S). These pharmacological data in C57BL/6 WT and α6L9S mice strongly support the hypothesis that MHbVI, but not MHbVL, neurons express functional, high-sensitivity α6* nAChRs.

MHb neurons fire spontaneous action potentials in slice preparation (Gorlich et al., 2013; Dao et al., 2014; Shih et al., 2014). To examine the effects of short-term nicotine exposure on MHbVL and MHbVI neuron firing rates, we recorded baseline and nicotine-elicited action potential firing. Using the cell-attached mode in recordings from MHbVL and MHbVI neurons, firing was recorded before, during, and after a 16-minute bath exposure to nicotine (1 μM). Although typical nicotine concentrations in the cerebrospinal fluid of smokers is ~300 nM, higher concentrations have been reported (Malkawi et al., 2009). Cell-attached recording was chosen to avoid disturbing the intracellular milieu. In addition, action potentials were recorded in the presence of a cocktail of inhibitors to block muscarinic receptors, type A gamma aminobutyric acid receptors, and glutamate receptors (1 μM atropine, 100 μM picrotoxin, and 10 μM 6-cyano-7-nitroquinoxaline-2,3-dione) to better isolate the actions of nAChRs. In three MHb neurons, the firing frequency at rest was not altered by these inhibitors (data not shown), suggesting that tonic action potential firing is driven by intrinsic factors and is independent of inputs releasing glutamate, gamma aminobutyric acid, or ACh. A recent study reached a similar conclusion regarding spontaneous firing in MHb neurons (Gorlich et al., 2013).

Neurons from MHbVL and MHbVI fired at a similar frequency at rest (MHbVL, 5.5 ± 0.6 Hz, $n = 9$; MHbVI, 4.5 ± 0.8 Hz, $n = 8$, $p = 0.3366$). MHbVL neurons increased their firing rate quickly in response to 1 μM nicotine, followed subsequently by attenuation of this increased firing in the continued presence of 1 μM nicotine (Fig. 3, A and B). In MHbVI, the pattern was different. In response to 1 μM nicotine, firing increased slower than in VL neurons (Fig. 3, A and B). In contrast to the attenuated firing seen in VL neurons, VI neurons exhibited sustained firing in the continued presence of 1 μM nicotine for the duration of the experiment (Fig. 3, A and B). We quantified action potential firing at three different time points during the experiment, and the results indicate a sustained increase for MHbVI cells at the end of the experiment (Fig. 3C; 8.2 ± 0.6 Hz, $p = 0.0002$ versus baseline). In contrast, in MHbVL cells the firing frequency was not different at the end of the experiment compared with the prenicotine firing rate (Fig. 3C; 6.1 ± 0.9 Hz, $p = 0.5252$ versus baseline). Together, these experiments reveal that nicotine has a differential ability to influence neuronal activity in MHbVL and MHbVI neurons. We next sought to determine whether nAChR desensitization accounted for these differences.

In experiments measuring action potential firing in ventral tegmental area (VTA) neurons, a biphasic response to nicotine was measured (Liu et al., 2012). This response consists of an early and brief phase, followed by a later, sustained firing response that is hypothesized to be related to the desensitization properties of nAChR subtypes in VTA neurons (Liu et al., 2012). We hypothesized that differences in nicotine-elicited action potential firing in MHbVL and MHbVI was due to differential desensitization properties of nAChRs in these areas. To test this hypothesis, whole-cell recordings were made from MHbVL and MHbVI neurons in the voltage clamp mode. Inward cation currents through nAChRs were induced by pressure application of ACh (100 μM, 250 milliseconds) at 3-minute intervals to promote stable responses before nicotine application. Similar to a previous study (Pidoplichko et al., 1997), we then tested the effect of a 15-minute nicotine (1 μM) application on the magnitude of these ACh-evoked currents. After 15 minutes of nicotine exposure, ACh puffs were resumed to determine whether there were any changes in current amplitude after nicotine exposure (Fig. 4A). After 15 minutes of nicotine application, responses to ACh were

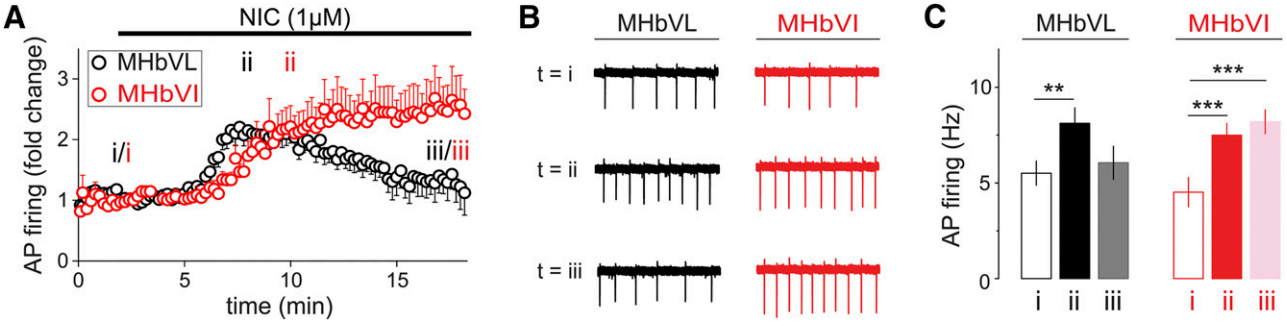

Fig. 3. Effect of prolonged nicotine application on firing rate as measured in cell-attached recordings in MHbVL and MHbVI. (A) Cell-attached recordings from MHbVL and MHbVI neurons were conducted. Baseline firing was recorded for several minutes, followed by superfusion of nicotine (1 μM) for 16 minutes. (B) Representative traces obtained in cell-attached mode in MHbVL and MHbVI cells. Each experiment comprised a recording taken at −60 mV, and the firing rates were calculated at time point *i* ($t = 2$ minutes, baseline), *ii* ($t = 8$ minutes for MHbVL, $t = 10$ minutes for MHbVI, peak response in 1 μM nicotine), and *iii* ($t = 18$ minutes, prolonged exposure). (C) Quantification of summary data shown in (B). Average firing rates at the indicated time points are shown. $^{**}p < 0.01$; $^{***}p < 0.001$ (paired *t* test).

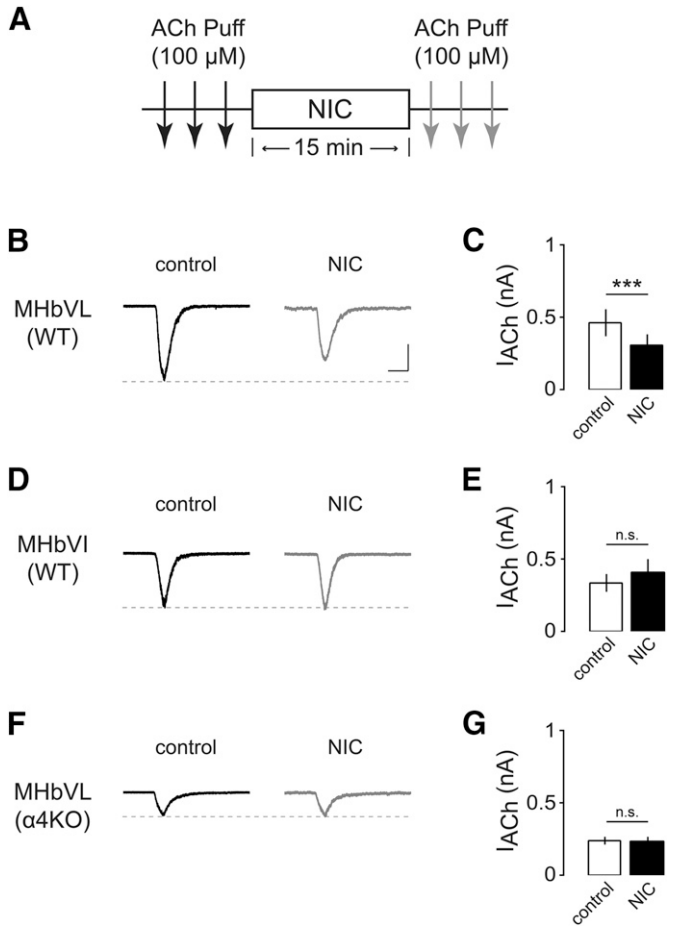

Fig. 4. Effects of acute nicotine on ACh-induced currents in MHbVL and MHbVI neurons. (A) Diagram of the experimental protocol. MHb neurons were held at −60 mV. Three ACh (100 μM) applications (each arrow is one application) prior to nicotine (1 μM) and three after 15-minute exposure to nicotine were conducted. (B) Representative inward currents induced by ACh application before (black trace) and after (gray trace) nicotine application to MHbVL neurons. Scale bar: 250 pA, 500 milliseconds. (C) Summary data showing nicotine-induced changes of nAChR-mediated peak currents in MHbVL neurons; ***$p < 0.001$ (paired t test). (D) Representative inward currents induced by ACh application before (black trace) and after (gray trace) nicotine application to MHbVI neurons. Scale bar: 250 pA, 500 milliseconds. (E) Summary data showing nicotine-induced changes of nAChR-mediated peak currents in MHbVI neurons. (F) Representative inward currents induced by ACh application before (black trace) and after (gray trace) nicotine application to MHbVL neurons of α4KO mice. Scale bar: 250 pA, 500 milliseconds. (G) Summary data showing nicotine-induced changes of nAChR-mediated peak currents in MHbVL neurons from α4KO mice.

reduced in MHbVL neurons (Fig. 4, B and C, 449.5 ± 79.1 and 286.7 ± 66.5 pA before and after 15-minute nicotine exposure, respectively, $n = 9$, $p = 0.0006$). However, 1 μM nicotine did not desensitize ACh-induced currents in MHbVI neurons receiving the same 15-minute exposure (Fig. 4, D and E, 345.1 ± 58.7 and 411.3 ± 90.5 pA before and after 15-minute nicotine exposure, respectively, $n = 6$, $p = 0.2396$). In both sets of experiments, there was a significant increase in RMS current noise after 15-minute nicotine compared with baseline before drug perfusion (2.8 ± 0.2 pA compared with 6.4 ± 0.3 pA, $p < 0.001$), which is an indication of increased nAChR activity (Drenan et al., 2008).

Desensitization is a common property of nAChRs, which are strongly influenced by subunit composition and stoichiometry. In other brain areas, nAChRs containing α4 and β2 subunits desensitize within seconds to a few minutes of exposure to physiologically relevant concentrations of nicotine (Pidoplichko et al., 1997). Receptors with α6 subunits appear to desensitize less than α4 (non-α6)* nAChRs (Grady et al., 2012). Previous studies have shown that neurons in the MHbVL express high levels of α4 receptors (Nashmi et al., 2007; Fonck et al., 2009; Shih et al., 2014). Accordingly, we hypothesized that MHbVL nAChRs exhibit stronger desensitization due to the presence of α4 subunits. To investigate this, we performed the same desensitization experiment (Fig. 4A) in α4KO mice. In MHbVL neurons from α4KO mice, ACh-induced inward currents were not diminished by a nicotine (1 μM) bath application (Fig. 4, F and G, 237.2 ± 26.0 and 234.2 ± 31.4 pA before and after 15-minute nicotine exposure, respectively, $n = 7$, $p = 0.8380$). Consistent with our prior work (Shih et al., 2014), peak currents were reduced in MHbVL neurons from α4KO mice relative to control mice (Fig. 4F). These data suggest that due to their specific expression in MHbVL cells, α4* nAChRs mediate desensitization and attenuated action potential firing following exposure to smoking relevant concentrations of nicotine.

Our data indicate that acute nicotine causes differential activation of nAChRs and differential firing responses in MHbVL and MHbVI. Chronic nicotine treatment alters nicotinic cholinergic signaling in the MHb to IPN pathway (Salas et al., 2004, 2009), and the acute mechanism we identified may play a role. To test our overall hypothesis that chronic exposure to nicotine differentially alters nAChR activity in subregions of MHb, we used a previously described protocol (Shih et al., 2014). Mice were implanted (subcutaneously) with nicotine-filled minipumps for 14 days, which delivered nicotine at 1 mg/kg per hour in C57BL/6J mice; this dose generates plasma levels of nicotine ~40 ng/ml (Sparks and Pauly, 1999). This concentration is comparable with nicotine plasma levels measured in the afternoon in smokers (Matta et al., 2007) (10–50 ng/ml of nicotine or 60–310 nM of nicotine). Control mice were implanted with minipumps filled with saline. After 14 days of chronic nicotine treatment, brain slices were prepared and recordings were made from MHbVL and MHbVI neurons (Fig. 5A). MHbVL neurons from mice treated with chronic nicotine displayed similar responses to puff-applied ACh (100 μM) compared with chronic saline control mice (saline: 520 ± 140.1 pA, $n = 6$; nicotine: 537 ± 130.2 pA, $n = 7$; $p = 0.8980$; Fig. 5, B and C). Conversely, chronic nicotine caused functional upregulation of nAChRs in MHbVI neurons; ACh-evoked inward currents were significantly enhanced by chronic nicotine treatment (saline: 439.5 ± 43.1 pA, $n = 13$; nicotine: 725.2 ± 77.7 pA, $n = 15$, $p = 0.0041$; Fig. 5, B and D).

Next, we sought to determine whether the functionally upregulated nAChRs in MHbVI neurons from mice treated chronically with nicotine are still resistant to desensitization similar to naïve MHbVI nAChRs (Fig. 3). Mice were implanted with minipumps delivering control saline or nicotine as described above. After 14 days, slices were prepared and whole-cell recordings were made from MHbVL and MHbVI neurons. ACh (100 μM) was puff applied before and after a bath application of 1 μM nicotine for 15 minutes. Recordings from MHbVL in both treatment groups displayed significant desensitization following 15 minutes of nicotine exposure (Fig. 6, A and B; saline: 479.9 ± 81.2 pA before acute nicotine and

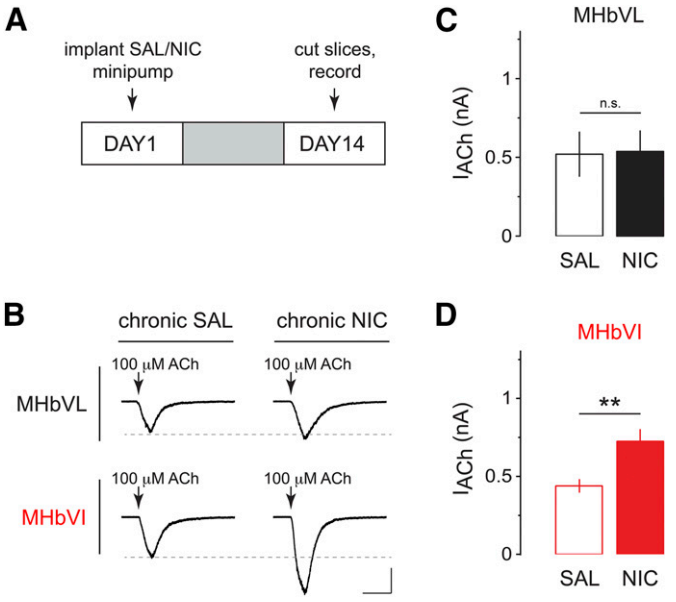

Fig. 5. Effects of chronic nicotine on ACh-induced currents in MHbVL and MHbVI neurons. (A) Nicotine dependence procedure. Mice were implanted with osmotic minipumps delivering either saline (SAL) or nicotine (NIC) (1 mg/kg per hour) for 14 days. On day 14, slices were prepared for electrophysiology. (B) Representative traces of ACh-evoked currents (100 μM, arrow) in MHbVL or MHbVI neurons from animals treated either with chronic SAL or chronic NIC. Inward current waveforms are an average of >2 traces. Scale bar: 250 pA, 500 milliseconds. (C) Scatter plot and grouped data of peak amplitude of ACh-evoked currents from MHbVL neurons from SAL- or NIC-treated mice. (D) Scatter plot and grouped data of peak amplitude of ACh-evoked currents from MHbVI neurons from SAL- or NIC-treated mice; *$p < 0.05$ (unpaired t test).

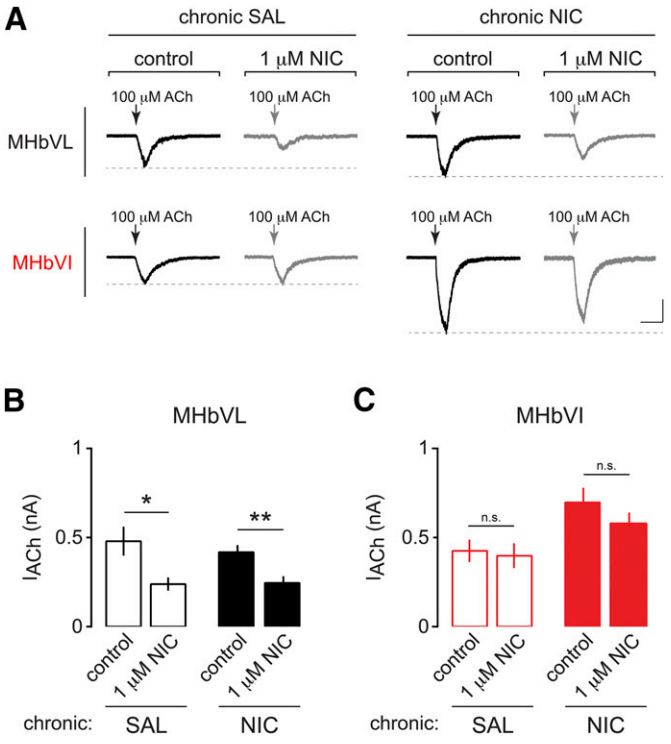

Fig. 6. Effects of chronic nicotine on desensitization of nAChRs in MHbVL and MHbVI cells exposed to acute nicotine. (A) Representative traces of ACh-evoked currents (100 μM, arrow) in MHbVL and MHbVI neurons from mice exposed to chronic saline (SAL) or chronic nicotine (NIC). Experiments were conducted as described in Fig. 4A: ACh (100 μM) was puff applied three times, nicotine (1 μM) was bath applied for 16 minutes, and ACh was applied three times again to the recorded cell. Scale bar: 200 pA, 500 milliseconds. (B) Summary data plot showing average current amplitude for 100 μM ACh-evoked responses in MHbVL neurons from mice treated chronically with SAL or NIC before (control) and after bath application of nicotine (NIC) (1 μM). *$p < 0.05$; **$p < 0.01$ (paired t test). (C) Summary data plot showing average current amplitude for 100 μM ACh-evoked responses in MHbVI neurons from mice treated chronically with SAL or NIC before (control) and after bath application of NIC (1 μM).

239.0 ± 37.2 pA after acute nicotine, $n = 7$, $p = 0.0156$; nicotine: 418.2 ± 39.9 pA before acute nicotine and 245.3 ± 37.3 pA after acute nicotine, $n = 9$, $p = 0.0053$). As with nAChRs in MHbVI neurons naïve to prior nicotine exposure, nAChRs in MHbVI neurons from mice treated chronically with saline or nicotine did not exhibit desensitization following an acute, bath application of nicotine (Fig. 6, A and B; saline: 425.7 ± 62.8 pA before acute nicotine and 398.3 ± 69.5 pA after acute nicotine, $n = 8$, $p = 0.4171$; nicotine: 696.9 ± 82.5 pA before acute nicotine and 579.9 ± 60.6 pA after acute nicotine, $n = 11$, $p = 0.1429$).

Finally, we sought to identify the functional consequences of chronic nicotine treatment on neuronal activity in MHbVL and MHbVI. Experiments were performed as described in Fig. 5A. Cell-attached patch clamp recordings were made in MHbVL and MHbVI neurons from mice treated chronically with nicotine or saline for 14 days. Recordings in MHbVL neurons revealed that basal firing was indistinguishable between chronic nicotine-treated and chronic saline-treated groups (Fig. 7, A and C; saline: 4.2 ± 0.8 Hz, $n = 6$; nicotine: 4.1 ± 0.3 Hz, $n = 17$; $p = 0.9359$) and that bath application of acute nicotine (1 μM) resulted in a similar increase of firing frequency in both groups (Fig. 7D; saline: 2.0 ± 0.2-fold increase, $n = 6$; nicotine: 1.8 ± 0.2-fold increase, $n = 6$; $p = 0.4679$). Also, the fold increase in MHbVL neuron action potential firing was the same as in untreated (no minipump implanted) mice (ANOVA: $p = 0.3461$). Remarkably, MHbVI neurons from mice treated chronically with nicotine displayed a sustained elevation in their baseline firing rates relative to MHbVI neurons from mice treated chronically with saline (Fig. 7, B and C; saline: 4.5 ± 0.7 Hz, $n = 9$; nicotine: 7.4 ± 0.6 Hz, $n = 14$; $p = 0.0064$). In contrast to MHbVL neurons, when MHbVI neurons from mice treated chronically with nicotine were exposed to acute nicotine (1 μM), there was no additional gain in action potential firing compared with MHbVI neurons from mice treated chronically with saline (Fig. 7D; saline: 2.1 ± 0.3-fold increase, $n = 6$; nicotine: 1.1 ± 0.1-fold increase, $n = 7$; $p = 0.0188$). Together, these results indicate that chronic nicotine selectively alters nAChR function and neuronal activity in different subregions of MHb.

Discussion

In this study, we sought to investigate subregions of MHb with regard to nAChR pharmacology and neuronal excitability using brain slice patch clamp electrophysiology. We determined that MHbVL and MHbVI subregions express pharmacologically distinct nAChRs. These distinct nAChRs respond differentially to both acute and chronic nicotine, and these differences directly translate into divergent action potential firing patterns in these MHb subregions.

Differential MHb nAChR Pharmacology. Our group and others have demonstrated high levels of $\alpha3$ and $\beta4$ nAChR

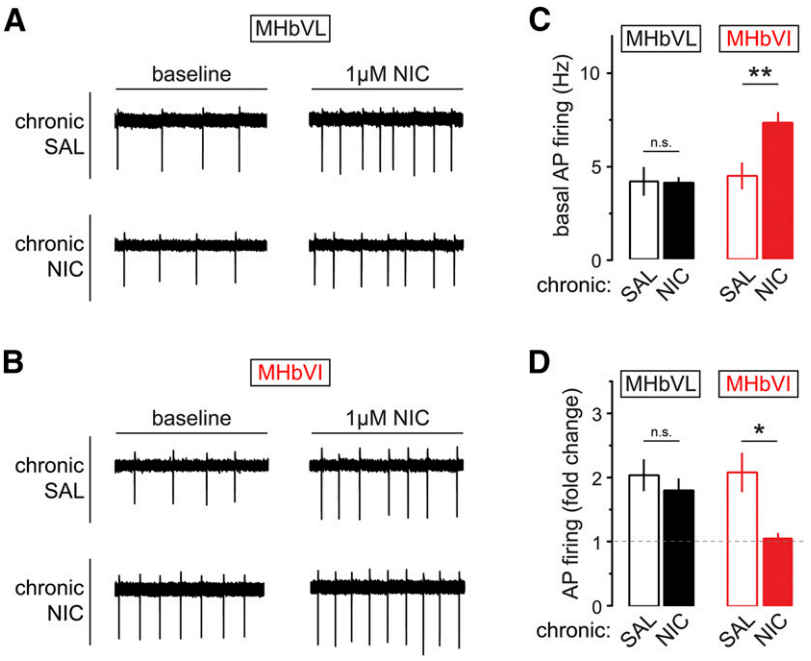

Fig. 7. Excitability changes in MHb neurons from mice exposed to chronic nicotine or saline. (A) Baseline and nicotine-elicited changes in MHbVL neurons after chronic nicotine (NIC) treatment. Representative cell-attached firing traces for MHbVL neurons showing the typical change in firing are shown for the four indicated conditions [chronic saline (SAL), baseline; chronic SAL, 1 μM nicotine; chronic NIC, baseline; chronic NIC, 1 μM nicotine]. (B) Baseline and nicotine-elicited changes in MHbVI neurons after chronic NIC treatment. Representative cell-attached firing traces for MHbVI neurons showing the typical change in firing are shown for the four indicated conditions (chronic SAL, baseline; chronic SAL, 1 μM nicotine; chronic NIC, baseline; chronic NIC, 1 μM nicotine). (C) Summary bar graph showing mean action potential firing rate at baseline for MHbVL and MHbVI neurons from mice treated with chronic SAL or chronic NIC; $^{**}p < 0.01$ (unpaired t test). (D) Summary bar graph showing mean fold change in action potential firing for nicotine-exposed (1 μM in bath for 15 minutes) MHbVL and MHbVI neurons from mice treated with chronic SAL or chronic NIC; $^{*}p < 0.05$ (unpaired t test).

subunit expression and function in all areas of ventral MHb (Quick et al., 1999; Shih et al., 2014). SR16584 antagonizes $\alpha3\beta4$ nAChRs and has little activity at $\alpha4\beta2$ and $\alpha7$ nAChRs (Zaveri et al., 2010). Thus, our data demonstrating that bath-applied SR16584 was effective at blocking ACh-evoked currents in both MHbVL and MHbVI are consistent with the prevailing notion that $\alpha3\beta4$* nAChRs play a dominant role in mediating nicotinic cholinergic signaling in MHb (Quick et al., 1999). Future pharmacological studies of SR16584s action at other nAChR subtypes will help confirm this suggestion. Although inward current responses attributed to MHbVL and MHbVI nAChRs were similar in overall sensitivity to puff-applied ACh (Fig. 1, C and D), there was a differential sensitivity to DHβE (Fig. 1, G and H). Although generally used to discriminate $\alpha7$ from $\beta2$* nAChRs in native preparations, DHβE has moderate antagonist activity at uncommon nAChR subtypes that may be present in MHb. For example, experiments using human nAChRs expressed in *Xenopus* oocytes showed that DHβE is a potent antagonist at $\alpha2\beta2$ and $\alpha4\beta4$ nAChRs (Chavez-Noriega et al., 1997). A wide array of nAChR subunits that are expressed in MHb cells, and responses evoked by 100 μM ACh are likely aggregate responses of multiple nAChR subtypes. Our DHβE data could reflect a slight sensitivity of multiple of these putative subtypes or it could reflect a complete block of a minor subtype and no antagonism of the others. More studies will be required to probe this question.

Our experiments (Fig. 2) utilizing αCtxMII, ACh applications, and α6L9S transgenic mice collectively support the idea that functional $\alpha6$* nAChRs are expressed in MHbVI neurons, but are excluded from MHbVL neurons. These findings are in line with our previous study using mouse strains expressing green fluorescent protein–tagged $\alpha6$ subunits, where $\alpha6$ subunit immunoreactivity was demonstrated in MHbVI cells (Shih et al., 2014). Our findings are similarly consistent with those of Henderson et al. (2014), who also demonstrated $\alpha6$ subunits in a subregion of MHb consistent with MHbVI.

Although nAChRs in MHbVL and MHbVI exhibited modest differences in response to acutely applied ACh, differences in their pharmacology was more pronounced when nicotine application was carried out. Nicotine-induced action potential firing was more rapid to reach the peak, but was attenuated in MHbVL cells. In contrast, firing developed more slowly and was more sustained in MHbVI cells (Fig. 3). The ability of the same nicotine treatment protocol to preferentially desensitize nAChRs in MHbVL (Fig. 4) may account for the differences in action potential firing we observed. $\alpha3\beta4$ nAChRs, although not especially sensitive to the desensitizing properties of nicotine (Fenster et al., 1997), are expressed throughout the ventral MHb and therefore may not explain the difference we observe. Rather, $\alpha4$ subunits in MHbVL may confer sensitivity to desensitization by nicotine, whereas the specific expression of $\alpha6$ subunits in MHbVI may confer resistance to desensitization. This supposition is supported by our data, showing that MHbVL nAChRs lacking $\alpha4$ subunits no longer desensitize in response to a 15-minute exposure to nicotine (Fig. 4, F and G). It is also supported by similar studies in VTA, another brain region expressing $\alpha4$ and $\alpha6$ subunits. Tapper et al. recently demonstrated that $\alpha6$-expressing neurons in VTA exhibit more sustained firing when exposed to nicotine in the bath (Liu et al., 2012). Marks et al. also demonstrated that $\alpha6$ subunits confer resistance to desensitization by nicotine (Grady et al., 2012). It should be noted that these cited studies concern $\alpha4$* and $\alpha6$* nAChRs that assemble with $\beta2$ subunits. It is not yet clear whether $\beta2$ subunits play a role in the differential desensitization that we observe in MHb. $\beta2$ Subunits are expressed in most areas of ventral MHb and account for a substantial fraction of nAChRs in both the mouse and rat (Grady et al., 2009; Shih et al., 2014).

Responses of MHb nAChRs and Neurons to Chronic Nicotine. In mice, chronic systemic nicotine treatment induces functional changes to nAChRs and/or neuronal circuits in the MHb to IPN pathway that is revealed by spontaneous or precipitated withdrawal approaches. Blockade of ongoing

nicotinic cholinergic signaling in the MHb of mice chronically exposed to nicotine triggers withdrawal, and specific nAChR subtypes play a role in this response (Salas et al., 2009). Our goal was to further study this activity of nicotine, and we identified MHbVI as a specific site that undergoes functional upregulation of nAChR activity in response to chronic nicotine (Fig. 5). These data are consistent with recent findings indicating that MHb α6 subunits, which are concentrated in MHbVI (Shih et al., 2014), upregulate following chronic nicotine treatment (Henderson et al., 2014). Conversely, we did not find nAChR activity to be functionally enhanced in MHbVL after chronic nicotine treatment (Fig. 5). This result is consistent with previous work showing that α4 subunits, which are concentrated in MHbVL (Shih et al., 2014), do not upregulate in response to chronic nicotine (Nashmi et al., 2007). Indeed, after 24 hours of withdrawal from chronic nicotine, responses attributed to α4 subunits exhibit *down-regulation* (Shih et al., 2014). Although these data and observations from the literature suggest that α6 upregulates in the MHbVI in our experiments, further electrophysiology studies will be necessary to probe this question. This is particularly important given that our pharmacological experiments suggest that nAChRs containing α6 subunits are a minority, although of high sensitivity, subtype in MHbVI. These results demonstrate the importance of considering MHb subregions independently when studying nAChRs and chronic nicotine, as several recent studies did not identify changes in the response of MHb neurons to nicotine when the MHb was analyzed without considering subregions (Gorlich et al., 2013; Hsu et al., 2013; Dao et al., 2014).

In addition to identifying changes in nAChR activity following chronic nicotine, we also connected these changes with alterations in action potential firing in MHb neurons exposed to nicotine. Chronic nicotine, but not chronic saline, caused an elevation in baseline action potential firing in MHbVI neurons (Fig. 7B). Likely as a consequence of enhanced baseline firing/excitability, acute nicotine was no longer able to further increase firing in our experiments (Fig. 7D). Thus, we have identified a specific neuron type that exhibits tolerance to acute nicotine exposure as a result of prior chronic exposure to nicotine. If our slice experiments are representative of MHbVI firing patterns in vivo, these data describe a potentially important change in MHb/IPN pathway circuit activity. Our recent data describing nAChR subunit expression/localization in the MHb/IPN pathway (Shih et al., 2014) confirm what was previously seen in anatomic studies (Contestabile and Flumerfelt, 1981): MHbVI projects to ventral IPN areas, whereas MHbVL projects more preferentially to dorsal IPN. It has recently become apparent that dorsal IPN neurons control somatic withdrawal responses (Zhao-Shea et al., 2013), and ventral IPN neurons control affective responses (Zhao-Shea et al., 2015). Moreover, during precipitated withdrawal from chronic nicotine exposure, MHb-derived inputs onto ventral IPN neurons control anxiety responses (Zhao-Shea et al., 2015). In our study, enhanced baseline firing and reduced nicotine-elicited firing in MHbVI neurons chronically exposed to nicotine is likely involved in activation of this affective withdrawal circuit in ventral IPN. Exerting specific control over MHbVI nAChRs and/or neuronal activity could be useful in modulating anxiety during nicotine withdrawal/cessation in human tobacco users.

Conclusion and Impact. The data we present here advance our knowledge of a key brain circuit involved in human nicotine intake, and future studies in rats or non-human primates should test our present conclusions in mouse models. We have shown previously (Shih et al., 2014) and in this study that MHb neurons and nAChRs are diverse in their pharmacology and activity patterns/excitability, respectively. As such, future mechanistic studies on the role of the MHb in nicotine addiction/withdrawal should discriminate between the various subregions that exist within the MHb. Because these different MHb subregions are known to project to different areas of IPN, and because these different areas of IPN mediate different aspects of nicotine withdrawal, these results may lead to a better understanding of nicotine dependence.

Acknowledgments

We thank members of the Drenan Laboratory for helpful insight and discussion.

Authorship Contributions

Participated in research design: Drenan, Shih.
Conducted experiments: Shih.
Contributed new reagents or analytic tools: McIntosh.
Performed data analysis: Drenan, Shih.
Wrote or contributed to the writing of the manuscript: Drenan, Shih.

References

Aizawa H, Kobayashi M, Tanaka S, Fukai T, and Okamoto H (2012) Molecular characterization of the subnuclei in rat habenula. *J Comp Neurol* **520**:4051–4066.
Azam L, Maskos U, Changeux JP, Dowell CD, Christensen S, De Biasi M, and McIntosh JM (2010) α-Conotoxin BuIA[T5A;P6O]: a novel ligand that discriminates between α6ß4 and α6ß2 nicotinic acetylcholine receptors and blocks nicotine-stimulated norepinephrine release. *FASEB J* **24**:5113–5123.
Bromberg-Martin ES, Matsumoto M, and Hikosaka O (2010) Dopamine in motivational control: rewarding, aversive, and alerting. *Neuron* **68**:815–834.
Cartier GE, Yoshikami D, Gray WR, Luo S, Olivera BM, and McIntosh JM (1996) A new α-conotoxin which targets α3β2 nicotinic acetylcholine receptors. *J Biol Chem* **271**:7522–7528.
Chavez-Noriega LE, Crona JH, Washburn MS, Urrutia A, Elliott KJ, and Johnson EC (1997) Pharmacological characterization of recombinant human neuronal nicotinic acetylcholine receptors hα2β2, hα2β4, hα3β2, hα3β4, hα4β2, hα4β4 and hα7 expressed in *Xenopus* oocytes. *J Pharmacol Exp Ther* **280**:346–356.
Cohen BN, Mackey ED, Grady SR, McKinney S, Patzlaff NE, Wageman CR, McIntosh JM, Marks MJ, Lester HA, and Drenan RM (2012) Nicotinic cholinergic mechanisms causing elevated dopamine release and abnormal locomotor behavior. *Neuroscience* **200**:31–41.
Contestabile A and Flumerfelt BA (1981) Afferent connections of the interpeduncular nucleus and the topographic organization of the habenulo-interpeduncular pathway: an HRP study in the rat. *J Comp Neurol* **196**:253–270.
Contestabile A, Villani L, Fasolo A, Franzoni MF, Gribaudo L, Oktedalen O, and Fonnum F (1987) Topography of cholinergic and substance P pathways in the habenulo-interpeduncular system of the rat. An immunocytochemical and microchemical approach. *Neuroscience* **21**:253–270.
Dani JA and Bertrand D (2007) Nicotinic acetylcholine receptors and nicotinic cholinergic mechanisms of the central nervous system. *Annu Rev Pharmacol Toxicol* **47**:699–729.
Dani JA and Harris RA (2005) Nicotine addiction and comorbidity with alcohol abuse and mental illness. *Nat Neurosci* **8**:1465–1470.
Dao DQ, Perez EE, Teng Y, Dani JA, and De Biasi M (2014) Nicotine enhances excitability of medial habenular neurons via facilitation of neurokinin signaling. *J Neurosci* **34**:4273–4284.
Drenan RM, Grady SR, Steele AD, McKinney S, Patzlaff NE, McIntosh JM, Marks MJ, Miwa JM, and Lester HA (2010) Cholinergic modulation of locomotion and striatal dopamine release is mediated by α6α4* nicotinic acetylcholine receptors. *J Neurosci* **30**:9877–9889.
Drenan RM, Grady SR, Whiteaker P, McClure-Begley T, McKinney S, Miwa JM, Bupp S, Heintz N, McIntosh JM, and Bencherif M et al. (2008) In vivo activation of midbrain dopamine neurons via sensitized, high-affinity α6 nicotinic acetylcholine receptors. *Neuron* **60**:123–136.
Engle SE, Broderick HJ, and Drenan RM (2012) Local application of drugs to study nicotinic acetylcholine receptor function in mouse brain slices. *J Vis Exp* e50034.
Engle SE, Shih PY, McIntosh JM, and Drenan RM (2013) α4α6β2* nicotinic acetylcholine receptor activation on ventral tegmental area dopamine neurons is sufficient to stimulate a depolarizing conductance and enhance surface AMPA receptor function. *Mol Pharmacol* **84**:393–406.

Fenster CP, Rains MF, Noerager B, Quick MW, and Lester RA (1997) Influence of subunit composition on desensitization of neuronal acetylcholine receptors at low concentrations of nicotine. *J Neurosci* **17**:5747–5759.

Fonck C, Nashmi R, Salas R, Zhou C, Huang Q, De Biasi M, Lester RA, and Lester HA (2009) Demonstration of functional α4-containing nicotinic receptors in the medial habenula. *Neuropharmacology* **56**:247–253.

Fowler CD, Lu Q, Johnson PM, Marks MJ, and Kenny PJ (2011) Habenular α5 nicotinic receptor subunit signalling controls nicotine intake. *Nature* **471**:597–601.

Frahm S, Slimak MA, Ferrarese L, Santos-Torres J, Antolin-Fontes B, Auer S, Filkin S, Pons S, Fontaine JF, and Tsetlin V et al. (2011) Aversion to nicotine is regulated by the balanced activity of β4 and α5 nicotinic receptor subunits in the medial habenula. *Neuron* **70**:522–535.

Görlich A, Antolin-Fontes B, Ables JL, Frahm S, Slimak MA, Dougherty JD, and Ibañez-Tallon I (2013) Reexposure to nicotine during withdrawal increases the pacemaking activity of cholinergic habenular neurons. *Proc Natl Acad Sci USA* **110**:17077–17082.

Grady SR, Moretti M, Zoli M, Marks MJ, Zanardi A, Pucci L, Clementi F, and Gotti C (2009) Rodent habenulo-interpeduncular pathway expresses a large variety of uncommon nAChR subtypes, but only the α3β4* and α3β3β4* subtypes mediate acetylcholine release. *J Neurosci* **29**:2272–2282.

Grady SR, Wageman CR, Patzlaff NE, and Marks MJ (2012) Low concentrations of nicotine differentially desensitize nicotinic acetylcholine receptors that include α5 or α6 subunits and that mediate synaptosomal neurotransmitter release. *Neuropharmacology* **62**:1935–1943.

Henderson BJ, Srinivasan R, Nichols WA, Dilworth CN, Gutierrez DF, Mackey ED, McKinney S, Drenan RM, Richards CI, and Lester HA (2014) Nicotine exploits a COPI-mediated process for chaperone-mediated up-regulation of its receptors. *J Gen Physiol* **143**:51–66.

Herkenham M and Nauta WJ (1977) Afferent connections of the habenular nuclei in the rat. A horseradish peroxidase study, with a note on the fiber-of-passage problem. *J Comp Neurol* **173**:123–146.

Hikosaka O (2010) The habenula: from stress evasion to value-based decision-making. *Nat Rev Neurosci* **11**:503–513.

Hilario MR, Turner JR, and Blendy JA (2012) Reward sensitization: effects of repeated nicotine exposure and withdrawal in mice. *Neuropsychopharmacology* **37**: 2661–2670.

Hsu YW, Tempest L, Quina LA, Wei AD, Zeng H, and Turner EE (2013) Medial habenula output circuit mediated by α5 nicotinic receptor-expressing GABAergic neurons in the interpeduncular nucleus. *J Neurosci* **33**:18022–18035.

Laviolette SR and van der Kooy D (2004) The neurobiology of nicotine addiction: bridging the gap from molecules to behaviour. *Nat Rev Neurosci* **5**:55–65.

Lester HA, Xiao C, Srinivasan R, Son CD, Miwa J, Pantoja R, Banghart MR, Dougherty DA, Goate AM, and Wang JC (2009) Nicotine is a selective pharmacological chaperone of acetylcholine receptor number and stoichiometry. Implications for drug discovery. *AAPS J* **11**:167–177.

Liu L, Zhao-Shea R, McIntosh JM, Gardner PD, and Tapper AR (2012) Nicotine persistently activates ventral tegmental area dopaminergic neurons via nicotinic acetylcholine receptors containing α4 and α6 subunits. *Mol Pharmacol* **81**:541–548.

Malkawi AH, Al-Ghananeem AM, de Leon J, and Crooks PA (2009) Nicotine exposure can be detected in cerebrospinal fluid of active and passive smokers. *J Pharm Biomed Anal* **49**:129–132.

Marks MJ, Burch JB, and Collins AC (1983) Effects of chronic nicotine infusion on tolerance development and nicotinic receptors. *J Pharmacol Exp Ther* **226**: 817–825.

Marks MJ, Pauly JR, Gross SD, Deneris ES, Hermans-Borgmeyer I, Heinemann SF, and Collins AC (1992) Nicotine binding and nicotinic receptor subunit RNA after chronic nicotine treatment. *J Neurosci* **12**:2765–2784.

Matsumoto M and Hikosaka O (2007) Lateral habenula as a source of negative reward signals in dopamine neurons. *Nature* **447**:1111–1115.

Matsumoto M and Hikosaka O (2009) Representation of negative motivational value in the primate lateral habenula. *Nat Neurosci* **12**:77–84.

Matta SG, Balfour DJ, Benowitz NL, Boyd RT, Buccafusco JJ, Caggiula AR, Craig CR, Collins AC, Damaj MI, and Donny EC et al. (2007) Guidelines on nicotine dose selection for in vivo research. *Psychopharmacology (Berl)* **190**:269–319.

McIntosh JM, Azam L, Staheli S, Dowell C, Lindstrom JM, Kuryatov A, Garrett JE, Marks MJ, and Whiteaker P (2004) Analogs of α-conotoxin MII are selective for α6-containing nicotinic acetylcholine receptors. *Mol Pharmacol* **65**:944–952.

Montone KT, Fass B, and Hamill GS (1988) Serotonergic and nonserotonergic projections from the rat interpeduncular nucleus to the septum, hippocampal formation and raphe: a combined immunocytochemical and fluorescent retrograde labelling study of neurons in the apical subnucleus. *Brain Res Bull* **20**:233–240.

Nashmi R, Xiao C, Deshpande P, McKinney S, Grady SR, Whiteaker P, Huang Q, McClure-Begley T, Lindstrom JM, and Labarca C et al. (2007) Chronic nicotine cell specifically upregulates functional α4* nicotinic receptors: basis for both tolerance in midbrain and enhanced long-term potentiation in perforant path. *J Neurosci* **27**: 8202–8218.

Pidoplichko VI, DeBiasi M, Williams JT, and Dani JA (1997) Nicotine activates and desensitizes midbrain dopamine neurons. *Nature* **390**:401–404.

Powers MS, Broderick HJ, Drenan RM, and Chester JA (2013) Nicotinic acetylcholine receptors containing α6 subunits contribute to alcohol reward-related behaviours. *Genes Brain Behav* **12**:543–553.

Qin C and Luo M (2009) Neurochemical phenotypes of the afferent and efferent projections of the mouse medial habenula. *Neuroscience* **161**:827–837.

Quick MW, Ceballos RM, Kasten M, McIntosh JM, and Lester RA (1999) α3β4 subunit-containing nicotinic receptors dominate function in rat medial habenula neurons. *Neuropharmacology* **38**:769–783.

Salas R, Pieri F, and De Biasi M (2004) Decreased signs of nicotine withdrawal in mice null for the β4 nicotinic acetylcholine receptor subunit. *J Neurosci* **24**: 10035–10039.

Salas R, Sturm R, Boulter J, and De Biasi M (2009) Nicotinic receptors in the habenulo-interpeduncular system are necessary for nicotine withdrawal in mice. *J Neurosci* **29**:3014–3018.

Salminen O, Drapeau JA, McIntosh JM, Collins AC, Marks MJ, and Grady SR (2007) Pharmacology of α-conotoxin MII-sensitive subtypes of nicotinic acetylcholine receptors isolated by breeding of null mutant mice. *Mol Pharmacol* **71**:1563–1571.

Shibata H and Suzuki T (1984) Efferent projections of the interpeduncular complex in the rat, with special reference to its subnuclei: a retrograde horseradish peroxidase study. *Brain Res* **296**:345–349.

Shih PY, Engle SE, Oh G, Deshpande P, Puskar NL, Lester HA, and Drenan RM (2014) Differential expression and function of nicotinic acetylcholine receptors in subdivisions of medial habenula. *J Neurosci* **34**:9789–9802.

Sparks JA and Pauly JR (1999) Effects of continuous oral nicotine administration on brain nicotinic receptors and responsiveness to nicotine in C57Bl/6 mice. *Psychopharmacology (Berl)* **141**:145–153.

Steinsland OS and Furchgott RF (1975) Desensitization of the adrenergic neurons of the isolated rabbit ear artery to nicotinic agonists. *J Pharmacol Exp Ther* **193**:138–148.

World Health Organization (2011) *Department of Mental Health and Substance Abuse, Global Status Report on Alcohol 2011*, World Health Organization Department of Mental Health and Substance Abuse, Geneva, Switzerland.

Yamaguchi T, Danjo T, Pastan I, Hikida T, and Nakanishi S (2013) Distinct roles of segregated transmission of the septo-habenular pathway in anxiety and fear. *Neuron* **78**:537–544.

Zaveri N, Jiang F, Olsen C, Polgar W, and Toll L (2010) Novel α3β4 nicotinic acetylcholine receptor-selective ligands. Discovery, structure-activity studies, and pharmacological evaluation. *J Med Chem* **53**:8187–8191.

Zhao-Shea R, DeGroot SR, Liu L, Vallaster M, Pang X, Su Q, Gao G, Rando OJ, Martin GE, and George O et al. (2015) Increased CRF signalling in a ventral tegmental area-interpeduncular nucleus-medial habenula circuit induces anxiety during nicotine withdrawal. *Nat Commun* **6**:6770.

Zhao-Shea R, Liu L, Pang X, Gardner PD, and Tapper AR (2013) Activation of GABAergic neurons in the interpeduncular nucleus triggers physical nicotine withdrawal symptoms. *Curr Biol* **23**:2327–2335.

Address correspondence to: Ryan M. Drenan, Purdue University, Department of Medicinal Chemistry and Molecular Pharmacology, 575 Stadium Mall Dr., West Lafayette, IN 47907. E-mail: drenan@purdue.edu